Crystallization of C_{60}-End-Capped Poly(ethylene oxide)s

X. D. Huang and S. H. Goh*

Department of Chemistry, National University of Singapore, 3 Science Drive 3, Singapore 117543, Singapore

Received August 25, 2000; Revised Manuscript Received February 14, 2001

ABSTRACT: The isothermal crystallization of poly(ethylene oxide) (PEO), single-C_{60}-end-capped PEO (FPEO), and double-C_{60}-end-capped PEO (FPEOF) has been evaluated using polarized optical microscopy (POM) and differential scanning calorimetry (DSC). Comparison studies were also made on a physical mixture of PEO and C_{60} with the same C_{60} content as in FPEO. Wide-angle X-ray diffraction experiments indicate that the crystal structures of the PEO fractions in all samples are identical. The equilibrium melting temperatures of FPEO and FPEOF are lower than that of PEO. Both the overall crystallization rate and the spherulite growth rate of C_{60}-end-capped PEO are markedly slower as compared to PEO, whereas there is no apparent change in the rates for PEO in the physical mixture. Kinetic analyses of the crystallization data from both DSC and POM agree quite well. The fold surface free energy of FPEO is of about 1.8 times larger than that of PEO, while that of FPEOF is about 2.5 times larger than that of PEO. This increase in fold surface free energy has been attributed to hindrance exerted by the bulky C_{60} end groups.

Introduction

An understanding of polymer crystallization kinetics is of importance in the study of many aspects of semicrystalline polymers such as the control of spherulitic size and the determination of fold surface free energy. The Avrami analysis of crystallization kinetics has been used widely in this aspect. Although the Avrami parameters obtained provide insight into macroscopic controlling factors, they do not provide a molecular description of polymer crystal growth. A more molecularly based analysis and one which connects to the reptation theory of polymer melt diffusion is the kinetic nucleation theory expounded by Hoffman et al. which defines three regions (regimes) of crystal growth. Generally, the crystallization of polymers has been investigated using polarized optical microscopy (POM) and differential scanning calorimetry (DSC), since the combination of these two techniques is able to provide both kinetic and thermodynamic parameters for the polymer system.

Poly(ethylene oxide) (PEO) possesses a relatively simple structure and is capable of packing into crystals. PEO has been one of the most extensively studied crystalline polymers. In particular, the melt−crystallization behavior of PEO fractions in its low-molecular-weight range is most interesting. Kovacs et al. have studied the crystal growth rates and morphology of PEO fractions crystallized from the melt using optical microscopy.[1−5] The low-molecular-weight PEO fractions crystallized from the melt at low supercooling form lamellar single crystals with chains either fully extended or folded a small integer number of times with the OH-terminated chain ends rejected onto the surface layers of the lamellae. A series of low-molecular-weight PEO (M_w = 3000) with different end groups (−OH, $-OCH_3$, $-O(CH_3)_3$, and $-OC_6H_5$) have been systematically studied by Cheng et al.[6,7] By increasing the size of the end group, not only does the transformation of the nonintegral folding chain to integral folding chain crystals become increasingly difficult but also the linear crystal growth is hampered.

In this paper, we will compare the crystallization behavior of PEO and C_{60}-end-capped PEO. [60]Fullerene (C_{60}) has received tremendous interest not only for its many promising applications but also for its unusual molecular structure and perfect spherical shape.[8,9] C_{60} is spherical with a diameter of about 1 nm and is highly hydrophobic. We have recently reported that the incorporation of C_{60} at the chain ends of PEO produces a significant hydrophobic effect on its complexation with poly(methacrylic acid).[10] Because of its large three-dimensional structure, it is very interesting to study the effect of C_{60} on the crystallization behavior of PEO.

Experimental Section

Materials and Samples. C_{60} (99.9% pure) was obtained from Peking University, China. Poly(ethylene glycol) monomethyl ether (PEO) was obtained from Aldrich; its number-average molecular weight (M_n) and polydispersity are 2200 and 1.07, respectively, determined by GPC. Poly(ethylene glycol) (PEG) was obtained from Aldrich; its M_n and polydispersity are 2500 and 1.07, respectively.

Single-C_{60}-end-capped poly(ethylene oxide) (FPEO) was prepared by cycloaddition reaction of monoazido-terminated poly(ethylene oxide) (starting from PEO) with C_{60}.[11] Double-C_{60}-end-capped poly(ethylene oxide) (FPEOF) was prepared following the same procedure as FPEO, using PEG as the starting material.[10] The molecular structures of PEO, FPEO, and FPEOF are shown in Scheme 1. For comparison purposes, a physical mixture of PEO and C_{60} with the same C_{60} content as FPEO was prepared. The mixture, denoted as PEOMF, was prepared by solution casting from a 5 mL chlorobenzene solution containing 23 mg of C_{60} and 77 mg of PEO. Glass transition temperatures (T_gs) of PEO, FPEO, and PEOMF are 198 K, while that of FPEOF is 215 K. All the samples were carefully dried under vacuum prior to investigation.

Wide-Angle X-ray Diffraction (WAXD). X-ray diffraction measurements (XRD) were carried out on a Simens D5005 diffractometer (40 kV, 30 mA) using Ni-filtered Cu Kα radiation in 0.02° step from 5° to 40° (in 2θ) with 1 s per step. The intensity of the diffracted X-ray from the samples was measured by a scintillation counter.

Differential Scanning Calorimetry: Isothermal Crystallization. The isothermal crystallization kinetics of PEO,

* To whom correspondence should be addressed.

10.1021/ma0014822 CCC: $20.00
Published on Web 04/13/2001

Scheme 1

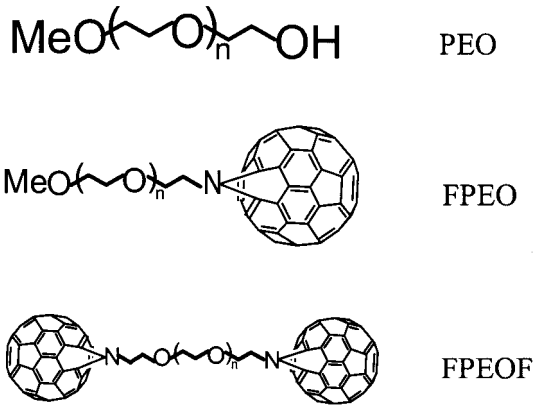

FPEO, FPEOF, and PEOMF were determined by monitoring the crystallization exotherm as a function of time at various crystallization temperatures (T_c). A Perkin-Elemer Pyris 1 DSC was used to monitor isothermal crystallization. Approximately 6 mg of sample was first heated to 100 °C and maintained at that temperature for 5 min to erase thermal history. The sample was then quenched to a specific T_c at a controlled cooling rate of 120 °C/min. The crystallization exotherm was then recorded as a function of time. The sample was kept at T_c for a sufficient period to allow complete crystallization. It was then heated to 100 °C at 20 °C/min to determine the melting temperature, T_m.

Polarized Optical Microscopy. The growths of PEO, FPEO, and PEOMF spherulites were observed with an Olympus BH2-UMA polarizing optical microscope, equipped with a Leitz Wetzlar hot stage and an Olympus exposure control unit. Sample sandwiched between two thin glass slides was melted for 5 min on a hot plate preheated to 100 °C. It was then quickly transferred onto the hot stage of the microscope which was maintained at a desired temperature (T_c). The sample was allowed to crystallize isothermally under crossed polars. The radial growth rate G ($G = dR/dt$) of the spherulites was measured by photographing the spherulites as a function of time during isothermal crystallization. The zero time was obtained by extrapolating the observed spherulite radius, R_t, to zero. The observed times were then "corrected" by subtracting this zero time from the experimental times.

Results and Discussion

WAXD and Equilibrium Melting Temperature. Figure 1 shows the wide-angle X-ray diffraction (WAXD) scans for PEO, FPEO, FPEOF, and PEOMF at room temperature. In all patterns there are two strong peaks occurring at the diffraction angle (2θ) of 19.1° and 23.2°, corresponding to 120 and 112/004 reflections from the PEO crystallites. Since the position of the Bragg diffraction peaks of FPEO or FPEOF do not shift significantly with respect to those of neat PEO, the incorporation of C_{60} produces no apparent change in unit cell dimensions and hence in crystal structure. Furthermore, no apparent signal of C_{60} crystal is observed in both polymers. However, for the physical mixture of C_{60} and PEO, signals of both PEO and C_{60} are observed. Thus, C_{60} is well dispersed in FPEO and FPEOF as the result of chemical connection.

Figure 2 shows the linear relationships between T_m's and T_c's in isothermal crystallization study for the four samples. The equilibrium melting points (T_m^0's) are determined by extrapolation to the line of $T_m = T_c$ according to the Hoffman−Weeks equation:[12]

$$T_m = \frac{1}{\gamma} T_c + \left(1 - \frac{1}{\gamma}\right) T_m^0 \qquad (1)$$

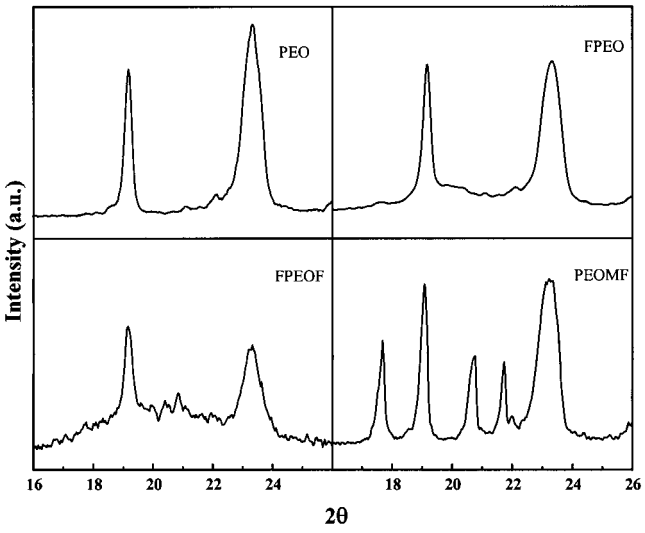

Figure 1. Wide-angle X-ray diffraction patterns of crystals of PEO, FPEO, FPEOF, and PEOMF.

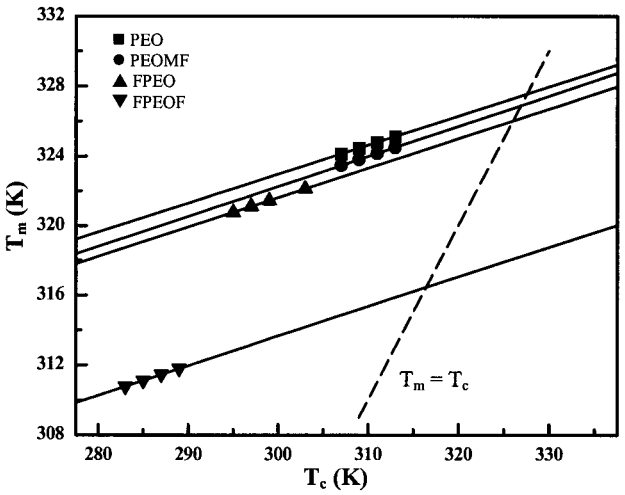

Figure 2. Hoffman−Weeks plots for PEO, PEOMF, FPEO, and FPEOF.

where γ is the ratio of the initial to the final lamellar thickness. The value of $1/\gamma$ is between 0 ($T_m = T_m^0$ for all T_c, in the case of most stable crystal) to 1 ($T_m = T_c$, in the case of inherently unstable crystal). In our cases, the value of $1/\gamma$ is about 0.17 for all samples, demonstrating that the stability of PEO crystal does not change upon the introduction of C_{60}. T_m^0 values of PEO, PEOMF, FPEO, and FPEOF are 54.6, 53.9, 53.0, and 43.4 °C, respectively. A depression of T_m^0 is observed upon the introduction of C_{60} into PEO, and the T_m^0 is depressed more dramatically for FPEOF where both ends of PEO are capped by C_{60}.

Polarized Optical Microscopy. Above the melting points, the cast-film samples of FPEO and FPEOF are optically clear and homogeneous but with a wine-red tint due to C_{60}. When observed with an optical microscope, the films were completely free of any haziness or heterogeneous domains. However, apparent heterogeneous domains of C_{60} were observed in the film of the physical mixture of PEO and C_{60}.

Figure 3 shows typical polarized micrographs for the isothermal crystallization of PEO, PEOMF, and FPEO at certain times after quenching to selected T_c's. The positive Maltese cross extinction pattern is evident, indicating perpendicular or parallel orientation of the

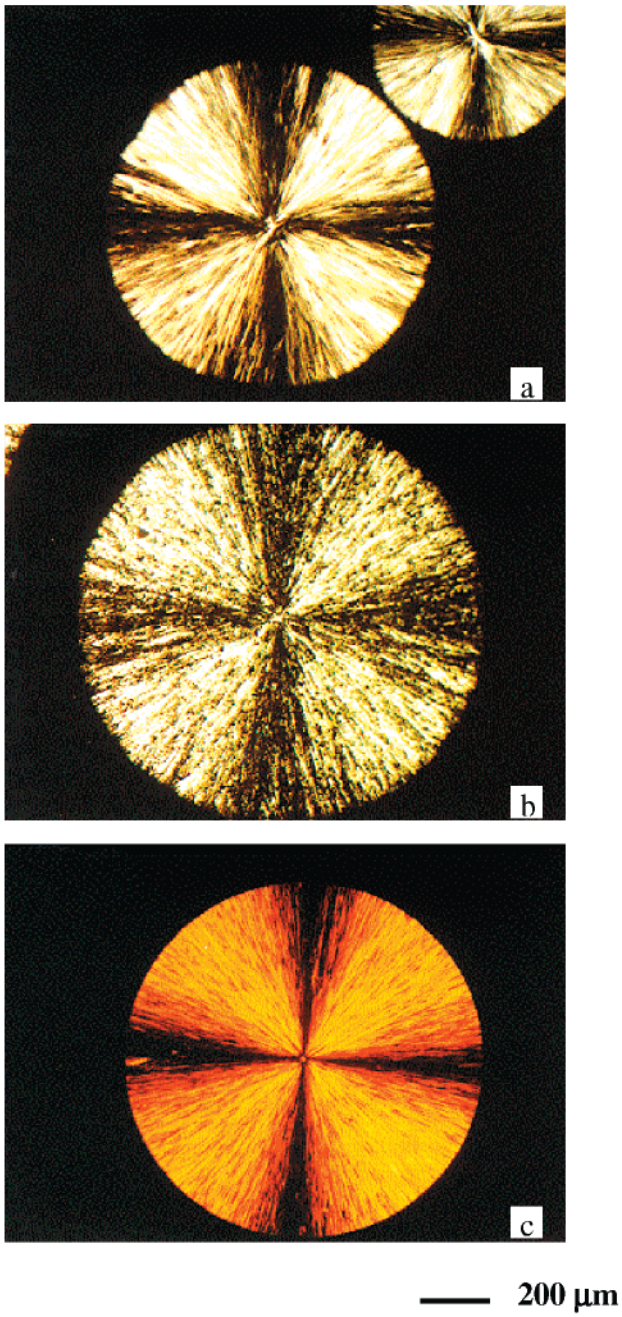

Figure 3. Typical polarized micrographs of spherulites of PEO (a), PEOMF (b), and FPEO (c).

crystalline molecule axis with respect to the spherulitic radius. Many black dots are evident on the micrographs of PEOMF due to phase separation of C_{60} and PEO. For the FPEOF sample, no apparent pattern was observed under polarized microscope. The spherulites could be too small to observe and/or the growth rate was too slow for observation under our experimental conditions. Nevertheless, the end-capping of C_{60} at both ends affects the crystallization significantly, and the crystallization kinetic data of FPEOF cannot be obtained from POM experiments.

For the three samples, the spherulitic radius increases linearly with time at all T_c's, and the growth rate decreases with increasing T_c. Furthermore, the induction time for nucleation becomes more protracted at higher T_c's. The spherulitic growth rate was determined from the gradient of the spherulitic radius vs time plot. The rate of crystallization of FPEO is greatly reduced (a 120-fold decrease in G at $\Delta T = 19$ K), and the difference increases with increasing T_c. The same trend has been observed by Cheng et al. for phenoxy-end-capped PEO.[7] Donth et al.[13] have demonstrated that mobile free ends are required during crystallization. Thus, the observed large reduction in spherulitic growth rate can be attributed to an effective halving of the crystallizable mobile ends in FPEO. For the physical mixture of PEO and C_{60}, there was no marked difference in the spherulitic texture as compared to that of PEO, as there is no change on the ends of crystallizable PEO chain.

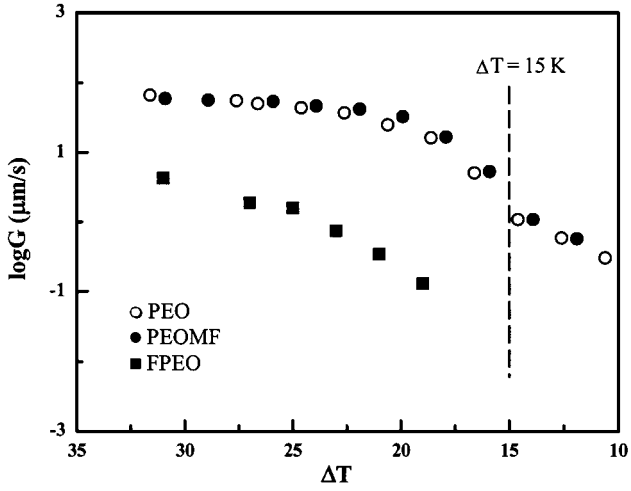

Figure 4. Relationship between logarithmic linear crystal growth rate (log G) of PEO, PEOMF, and FPEO crystallized from the melt and supercooling (ΔT).

Figure 4 represents the relationship between the logarithmic crystal growth rate and supercooling (ΔT) for PEO, FPEO, and PEOMF. For PEO and PEOMF, there are two individual growth rate curves separated by a crossover point. The intersecting point corresponds to a supercooling around 15 K, indicated by the vertical broken line in the figure.

Spherulitic growth kinetics can be analyzed using the kinetic nucleation theory expounded by Hoffman et al.[14−18] Three regions of crystal growth are predicted by this theory, the kinetics of each being controlled by the competition between nucleation and growth. In regime I, a single nucleation takes place on the substrate surface and leads to the substrate length being completely covered by a crystallization growth layer. At a lower temperature (a large supercooling, ΔT), regime II growth prevails where multiple nucleation takes place on the substrate. At still larger values of ΔT, regime III is entered where nucleation on the substrate is so prolific that the distance between niches approximates to a stem width. For each of these regimes, the crystal growth rate is expressed by

$$G(i) = G_0(\Delta T) \exp\left(\frac{-U^*}{R(T_c - T_\infty)}\right) \exp\left(\frac{-K_g(i)}{T_c \Delta T f}\right) \quad (2)$$

where i = I, II, or III, ΔT is the degree of supercooling ($T_m^0 - T_c$) with T_m^0 the equilibrium melting temperature and T_c the crystallization temperature, U^* is the activation energy of reeling in the polymer molecule from its melt reptation tube, T_∞ is the temperature below which this type of transportation ceases (taken here as $T_g - 30$ K), and f is a temperature correction

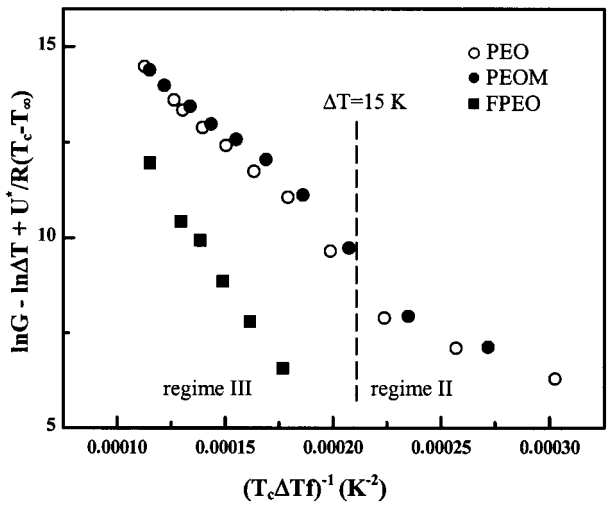

Figure 5. Hoffman−Lauritzen plots for PEO, PEOMF, and FPEO.

factor accounting for the change of melting enthalpy with temperature and is given by $2T_c/(T_m^0 + T_c)$. The preexponential term G_0 has been defined as $Z/n^{1+\lambda}$, which introduces the mobility, diffusion, or jump rate effect, and n is the degree of polymerization. The value of λ is defined as $n/2\phi$, where ϕ is the angle of sweep in radians of the first chain after it has achieved its first attachment. Each regime has a nucleation constant $K_g(i)$:

$$K_g(i) = \frac{nb_0\sigma\sigma_e T_m^0}{\Delta H_f k} \tag{3}$$

where σ is the lateral surface free energy, σ_e is the fold surface free energy, which is related to the difficulty of the chain to perform folding during crystallization, b_0 is the molecular thickness, k is the Boltzmann constant, ΔH_f is the heat of fusion per crystal unit volume, and n is a constant reflecting the regime of crystallization ($n = 4$ for regime I and III, and $n = 2$ for regime II).

Taking the logarithm of eq 2, one obtains

$$\ln G - \ln(\Delta T) + \frac{U^*}{R(T_c - T_\infty)} = \ln G_0 - \frac{K_g}{fT_c\Delta T} \tag{4}$$

Evaluation of the left-hand side of eq 4 requires values of T_g and U^* for PEO. The T_g value used here is 198 K, and U^* is 29.3 kJ mol^{-1}.[5,19] A plot of $\ln G - \ln(\Delta T) + U^*/R(T_c - T_\infty)$ vs $1/T_c(\Delta T)f$ can thus provide the values of K_g and G_0 for each regime.

Figure 5 clearly shows that two regimes are evident for PEO whereas for FPEO only one growth regime prevails over the range of T_c investigated here. For PEO, the ratio of the slopes of the two regions indicates that when $\Delta T > 15$ K, regime III growth takes place and when $\Delta T < 15$ K regime II growth is evident. Cheng et al.[19] reported that for pure PEO regime II growth takes place for supercoolings between 10 and 17.5 K, and regime III growth takes place at larger supercoolings. Regime I growth appears to be confined to a very narrow range of ΔT between 8.5 and 10 K. Our data do conform to the behavior observed by Cheng et al. We did not study the crystallization at T_c higher than 44 °C as the induction time would be very long. Cheng et al. used the seeding procedure of Kovacs for their study at these temperatures. For FPEO, because of the relatively high supercooling (>17.5 °C), crystallization might have taken place only in regime III.

Table 1. Kinetic Data of PEO, PEOMF, and FPEO from POM Studies

polymer	regime	K_g (10^4 K^{-2})	$\sigma\sigma_e$ (10^{-6} J^2 m^{-4})	σ_e (10^{-3} J m^{-2})	q (kJ mol^{-1})	K_g(III)/K_g(II)
PEO	II	2.4	232	23.2	6.0	2.1
	III	5.0	243	24.3	6.3	
PEOMF	II	2.2	214	21.4	5.5	2.2
	III	4.8	231	23.1	6.0	
FPEO	III	8.7	421	42.1	10.8	

Detailed data on the K_g values, the products of lateral and folding surface free energies $\sigma\sigma_e$, the ratios between two regimes, and other parameters for PEO, PEOMF, and FPEO are listed in Table 1. It is evident that the K_g value of FPEO is 1.7 times larger than that of PEO. For the calculation of $\sigma\sigma_e$ from these K_g values, we have used a value of 4.62 Å for b_0 and $\Delta H_f = 2.13 \times 10^8$ J m^{-3} as reported in the literature.[20,21] The $\sigma\sigma_e$ value for the neat PEO is 243×10^{-6} J^2 m^{-4}, which agrees well with the results of other authors. Using the empirical relation $\sigma = 0.1b_0\Delta H_f = 10 \times 10^{-3}$ J m^{-2}, σ_e is calculated as shown in Table 1. For PEO the σ_e value is in good agreement with those reported by Kovacs[1−5] and Cheng.[19] It is very interesting that the fold surface energy σ_e increases about 1.7 times when one end is capped with C_{60}, indicating that chain folding is much more difficult in FPEO. Cheng et al. have observed that σ_e of phenoxy-end-capped PEO is about 1.3 times higher than that of PEO.[7] The work of chain folding is obtained directly from the fold surface free energy as

$$q = 2\sigma_e A \tag{5}$$

where A is the molecular cross-sectional area, which is 0.214 nm^2 for PEO. The q values for PEO, FPEO, and PEOMF are also listed in Table 1. q is closely related to chain structure and is approximately proportional to chain stiffness. For FPEO, q is 1.7 times larger than that for PEO, demonstrating that the huge C_{60} makes chain stiffer and imposes a greater hindrance on the folding of PEO chain.

Differential Scanning Calorimetry: Avrami Analysis. We have used the enthalpies of fusion data from DSC to perform Avrami analysis. For brevity, only the DSC curves of FPEOF at various crystallization temperatures are shown in Figure 6. The Avrami analysis of isothermal crystallization kinetics was originally developed for metals[22−24] and later modified, for example, by Evans[25] and others, for polymers. The resultant equation is

$$1 - X(t) = \exp(-K_n t^n) \tag{6}$$

$X(t)$ is the relative crystallinity which was calculated from the DSC isothermal exotherm as

$$X(t) = \frac{\int_0^t (dQ/dt)\, dt}{\int_0^\infty (dQ/dt)\, dt} \tag{7}$$

where dQ/dt is the heat flow rate. K_n is the overall rate constant for the crystallization process. While K_n provides a quantitative check on the course of crystallization, the Avrami exponent, n, provides qualitative information on the nature of the nucleation and growth process. Theoretically, the case $n = 4$ can only result

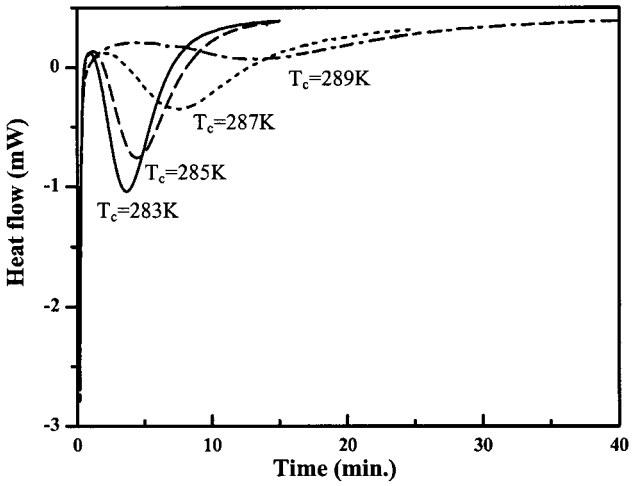

Figure 6. Isothermal DSC curves for FPEOF at different T_c's.

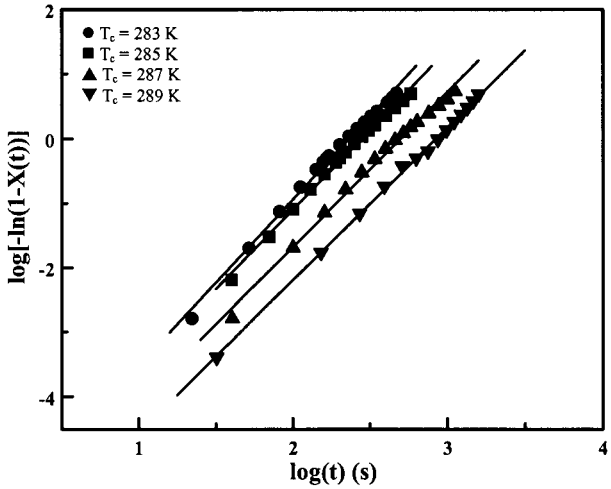

Figure 7. Avrami analysis for FPEOF.

from spherulitic growth from sporadic nuclei (homogeneous nucleation), whereas $n = 3$ can result both from spherulitic growth of instantaneous nuclei (heterogeneous nucleation) or disklike (lamellar) growth from sporadic nuclei. The analysis involves plotting $\log[-\ln(1 - X(t))]$ as a function of $\log t$ and determining n from the initial slope and K_n from the intercept. Deviations from the Avrami analysis, that is, nonlinearities in the plot or fractional exponents, can in principle result from (i) simultaneous growth of two different types of spherulites or (ii) a single structure obtained from growth of two types of nuclei (homogeneous and heterogeneous).

Figure 7 shows the double-logarithmic plots for the Avrami analysis of enthalpy of fusion data for FPEOF. For the four PEO samples, the Avrami exponent ranges from 2.3 to 2.7, but no systematic variation of n with composition or temperature is found, indicating that the crystal growth control mechanism is nearly the same for all samples. Furthermore, the Avrami exponent is close to 3, demonstrating that the process might be spherulitic growth of instantaneous nuclei (heterogeneous nucleation).

Figure 8 shows K_n's obtained from the Avrami analysis plotted as a function of the supercooling for PEO, PEOMF, FPEO, and FPEOF. The overall crystallization rate constant K_n is a combination of nucleation and crystal growth rates. If the nucleation is instantaneous, the linear growth rate G is related to K_n by the simple

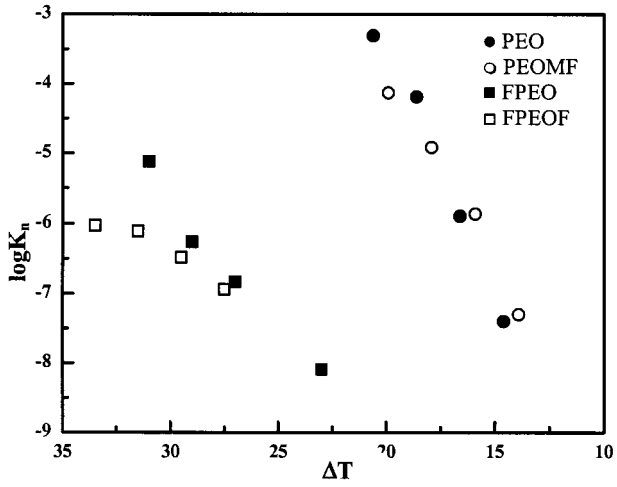

Figure 8. log K_n values obtained from Avrami analysis as a function of ΔT for PEO, PEOMF, FPEO, and FPEOF.

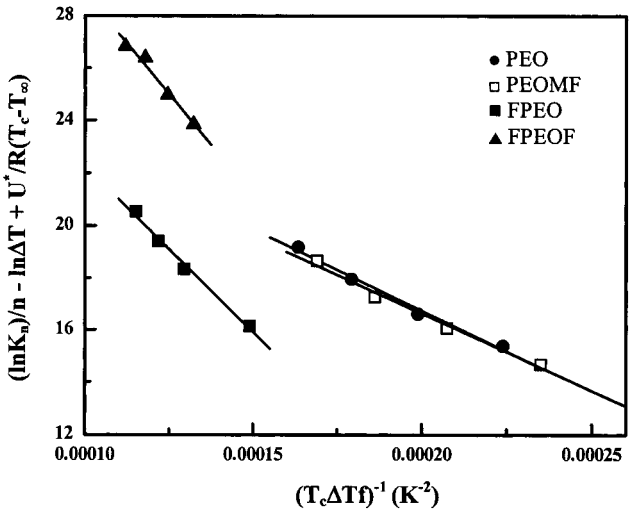

Figure 9. Plots of $(\ln K_n)/n - \ln \Delta T + U^*/R(T_c - T_\infty)$ vs $(T_c \Delta T f)^{-1}$ for PEO, PEOMF, FPEO, and FPEOF.

Table 2. Kinetic Data of PEO, PEOMF, FPEO, and FPEOF from DSC Studies

polymer	K_g(III) (10^4 K^{-2})	$\sigma\sigma_e$ (10^{-6} J^2 m^{-4})	σ_e (10^{-3} J m^{-2})	q (kJ mol^{-1})
PEO	6.3	302	30.2	7.8
PEOMF	5.9	285	28.5	7.5
FPEO	11.2	542	54.2	14
FPEOF	15.4	770	77.0	19.8

relation $G \propto K_n^{1/n}$ where n is the Avrami exponent.[26] Equation 4 can be rewritten as follows:

$$\frac{1}{n}\ln K_n - \ln(\Delta T) + \frac{U^*}{R(T_c - T_\infty)} = \ln(A_0) - \frac{K_g}{f\,T_c \Delta T} \tag{8}$$

The analysis of the experimental data has been made according to eq 8. As all data were from a supercooling temperature larger than 15 K, regime III may occur and was analyzed. As shown in Figure 9, good linear relationships were obtained. The K_g values were calculated from the slopes and are shown in Table 2 together with the corresponding estimated values for the fold surface free energies σ_e and q values. These values agree quite well with those obtained from POM study. The q value of FPEO is 1.8 times that of PEO while that of

FPEOF is 2.5 times that of PEO. It is therefore demonstrated that the incorporation of C_{60} at the chain end makes the PEO chain stiffer and more difficult to fold in the process of crystallization.

Conclusions

The introduction of C_{60} at the end of poly(ethylene oxide) chain results in a dramatic reduction in the overall crystallization rates. Regime analysis reveals that the fold surface free energy shows about 1.8 times increase for FPEO and 2.5 times increase for FPEOF compared to that of PEO. The increase of fold surface free energies has been attributed to the stiffening effect exerted by the bulky C_{60} end groups.

Acknowledgment. The authors thank the National University of Singapore for financial support of this research and Prof. Neal Chung for the use of thermal analysis facility in his laboratory.

References and Notes

(1) Kovacs, A. J.; Gonthier, A. *Kolloid Z. Z. Polym.* **1972**, *250*, 530.
(2) Kovacs, A. J.; Gonthier, A.; Straupe, C. *J. Polym. Sci., Polym. Symp.* **1975**, *50*, 283.
(3) Kovacs, A. J.; Straupe, C.; Gonthier, A. *J. Polym. Sci., Polym. Symp.* **1977**, *59*, 31.
(4) Kovacs, A. J.; Straupe, C. *Faraday Discuss. Chem. Soc.* **1979**, *68*, 225.
(5) Kovacs, A. J.; Straupe, C. *J. Cryst. Growth* **1980**, *48*, 210.
(6) Cheng, S. Z. D.; Chen, J.; Zhang, A.; Heberer, D. P. *J. Polym. Sci., Part B: Polym. Phys.* **1991**, *29*, 299.
(7) Cheng, S. Z. D.; Wu, S. S.; Chen, J.; Zhuo, Q.; Quirk, R. P.; von Meerwall, E. D.; Hsiao, B. S.; Habenschuss, A.; Zschack, P. R. *Macromolecules* **1993**, *26*, 5105.
(8) Hirsch, A. *The Chemistry of the Fullerenes*; Georg Thieme Verlag: Stuttgart, 1994.
(9) Taylor, R. *The Chemistry of Fullerenes*; World Scientific Publishing Co. Pte. Ltd.: Singapore, 1995.
(10) Huang, X. D.; Goh, S. H. *Macromolecules* **2000**, *33*, 8894.
(11) Huang, X. D.; Goh, S. H.; Lee, S. Y. *Macromol. Chem. Phys.* **2000**, *201*, 2660.
(12) Hoffman, J. D.; Weeks, J. J. *J. Res. Natl. Bur. Stand.* **1962**, *66A*, 13.
(13) Donth, E.; Kretzschmar, H.; Schulze, G.; Grag, D.; Höring, S.; Ulbricht, J. *Acta Polym.* **1987**, *38*, 261.
(14) Hoffman, J. D.; Davis, G. T.; Lauritzen, J. I., Jr. In *Treatise on Solid-State Chemistry*; Hannay, N. B., Ed.; Plenum Press: New York, 1976; Vol. 3, Chapter 7.
(15) Hoffman, J. D. *Faraday Discuss. Chem. Soc.* **1979**, *68*, 386.
(16) Hoffman, J. D. *Polymer* **1982**, *23*, 656.
(17) Hoffman, J. D. *Polymer* **1983**, *24*, 3.
(18) Hoffman, J. D.; Miller, R. L. *Macromolecules* **1988**, *21*, 3038.
(19) Cheng, S. Z. D.; Chen, J.; Janimak, J. J. *Polymer* **1990**, *31*, 1018.
(20) Godovsky, Y. K.; Slonimsky, G. L.; Garbar, N. M. *J. Polym. Sci., Part C* **1972**, *38*, 1.
(21) Calahorra, E.; Cortazar, M.; Guzmán, G. M. *Polymer* **1982**, *23*, 1322.
(22) Avrami, M. J. *Chem. Phys.* **1939**, *7*, 1103.
(23) Avrami, M. J. *Chem. Phys.* **1940**, *8*, 212.
(24) Avrami, M. J. *Chem. Phys.* **1941**, *9*, 177.
(25) Evans, U. R. *Trans. Faraday Soc.* **1945**, *41*, 365.
(26) Mandelkern, L. *Crystallization in Polymers*; McGraw-Hill: New York, 1964.

MA0014822